Micromagnetic simulation of thickness-dependent magnetization reversal processes in elongated iron nanodots

Micromagnetic simulation of thickness-dependent magnetization reversal processes in elongated iron nanodots

D Sudsom[1], C Döpke[1], T Blachowicz[2], A Ehrmann[1]
[1] Faculty of Engineering and Mathematics, Bielefeld University of Applied Sciences, 33619 Bielefeld, Germany
[2] Institute of Physics – Center for Science and Education, Silesian University of Technology, 44-100 Gliwice, Poland

E-mail: andrea.ehrmann@fh-bielefeld.de

Abstract. Micromagnetic simulations were used to investigate magnetization reversal processes in elongated ferromagnetic nanodots, prepared by combining two half-circles with a rectangle. The micromagnetic simulation program OOMMF is based on dynamically solving the Landau-Lifshitz-Gilbert equation of motion. Material parameters were chosen as typical for Fe (iron). Lateral dimensions were in most simulations chosen as 730 nm x 133 nm, while the dot height was varied between 3 nm and 54 nm. For different in-plane angles of the external magnetic field, varying magnetization reversal processes were found with changing dot thickness, offering a possibility to tailor magnetic states by modifying the thickness of the nanodot.

1. Introduction

Magnetic nanostructures offer interesting effective magnetic anisotropies due to the interplay between shape and magneto-crystalline anisotropy [1]. Such nanostructures can help principally understanding magnetization reversal processes on the nanoscale, e.g. by showing transitions between different magnetic states for different dimensions and materials or by realizing special effects like an exchange bias using core-shell structures [2-6].

Especially iron (Fe) shows interesting magnetization reversal processes when prepared in the form of nanodots [7,8] or open structures [9]. The latter often show flux-closed vortex states with strongly reduced stray fields [10,11]. In addition, nanodots or nano-frames may also give rise to multiple magnetic states at remanence [12,13] which can be used for novel data storage architectures or new logic elements [14].

Another important shape is represented by magnetic nanowires which can, e.g., be used in the Racetrack memory or similar technologies to store and manipulate data [15-17]. Depending on their dimensions, they also offer interesting magnetization reversal processes [18] and possibilities to transfer data by moving domain walls [19,20].

Here we report on micromagnetic simulations of a combination of rectangular, or nanowire-like, structures with nanodots, represented by Fe nanodots extended by a rectangular part between both halves. We investigate the magnetization reversal process which was shown to strongly depend on the lateral dimensions and the thickness of square and round Fe nanodots [7,8] for different angles with respect to the external magnetic field. This study can be regarded as a base for future simulations of

similar systems with varying sample thickness and dimensions, using the half-balls at the ends as a possibility to introduce domain walls [21,22].

2. Methods

The micromagnetic simulations described here were performed with the Object Oriented MicroMagnetic Framework (OOMMF) [23] which is based on dynamically solving the Landau-Lifshitz-Gilbert (LLG) equation of motion. The material iron was implemented by usual literature values: magnetization at saturation $M_S = 1700 \cdot 10^3$ A/m, exchange constant $A = 21 \cdot 10^{-12}$ J/m, magneto-crystalline anisotropy constant $K_1 = 48 \cdot 10^3$ J/m³ [24]. The Gilbert damping constant was set to $\alpha = 0.5$ to simulate a quasi-static case.

The lateral dimensions of the nanoparticle under investigation (Fig. 1) are 730 nm x 133 nm, while the dot height was varied between 3 nm and 54 nm (kept constant in each sample). Meshing was done with a cell size of 3 nm.

Figure 1. Shape of the magnetic nanodot under investigation.

Sample orientations are defined with respect to the horizontal in Fig. 1. Here, results of simulations along 15°, 30° and 60° are shown. In the results, longitudinal magnetization components M_L and transverse magnetization components M_T are given, always referring to the magnetic field orientation.

3. Results and discussion

Some results of simulations under an angle of 15° to the external magnetic field are depicted in Figure 2, an angle which was found to offer steps in the hysteresis loops correlated with stable intermediate states in former investigations [25]. Such intermediate states are of large interest for the development of new data storage media with more than one bit per storage position.

With increasing thickness of the simulated nanoparticle, the coercive fields become larger, until this effect is saturated and reversed around 24 nm. For a thickness of 39 nm, first steps along the sides of the longitudinal and transverse hysteresis loops become visible. In the simulation of a particle thickness of 45 nm, there are already three steps on either side of the loops which become broader for the largest thickness under examination, i.e. 54 nm.

Such steps are typically correlated with domain wall processes or magnetization reversal via vortex formation [7-9]. The reversal visible for thinner particles can be attributed to single-domain switching of the whole particle's magnetization, as it is proposed by the Stoner-Wohlfarth model (a common model for single-domain ferromagnets) and often the case for elliptical particles [26]. As found in previous investigations of Fe nanoparticles, magnetization in thinner structures is preferably switched coherently, while thicker structures support formation of domains and vortices [7,8].

For an angle of 60°, Figure 3 shows generally a similar behaviour. Again, for the thinnest samples, the well-known Stoner-Wohlfarth-like coherent magnetization reversal is visible, while for a thickness of 36 nm, the first small steps can be recognized. Simulating a thickness of 39 nm, these steps become clearer visible, while magnetization reversal for samples of 45 nm and higher thickness occurs via three steps.

Opposite to the results of 15° orientation, here the coercive fields become larger and larger for thicker samples, apparently approaching a maximum value which is not reached within the extent of the recent series of simulations.

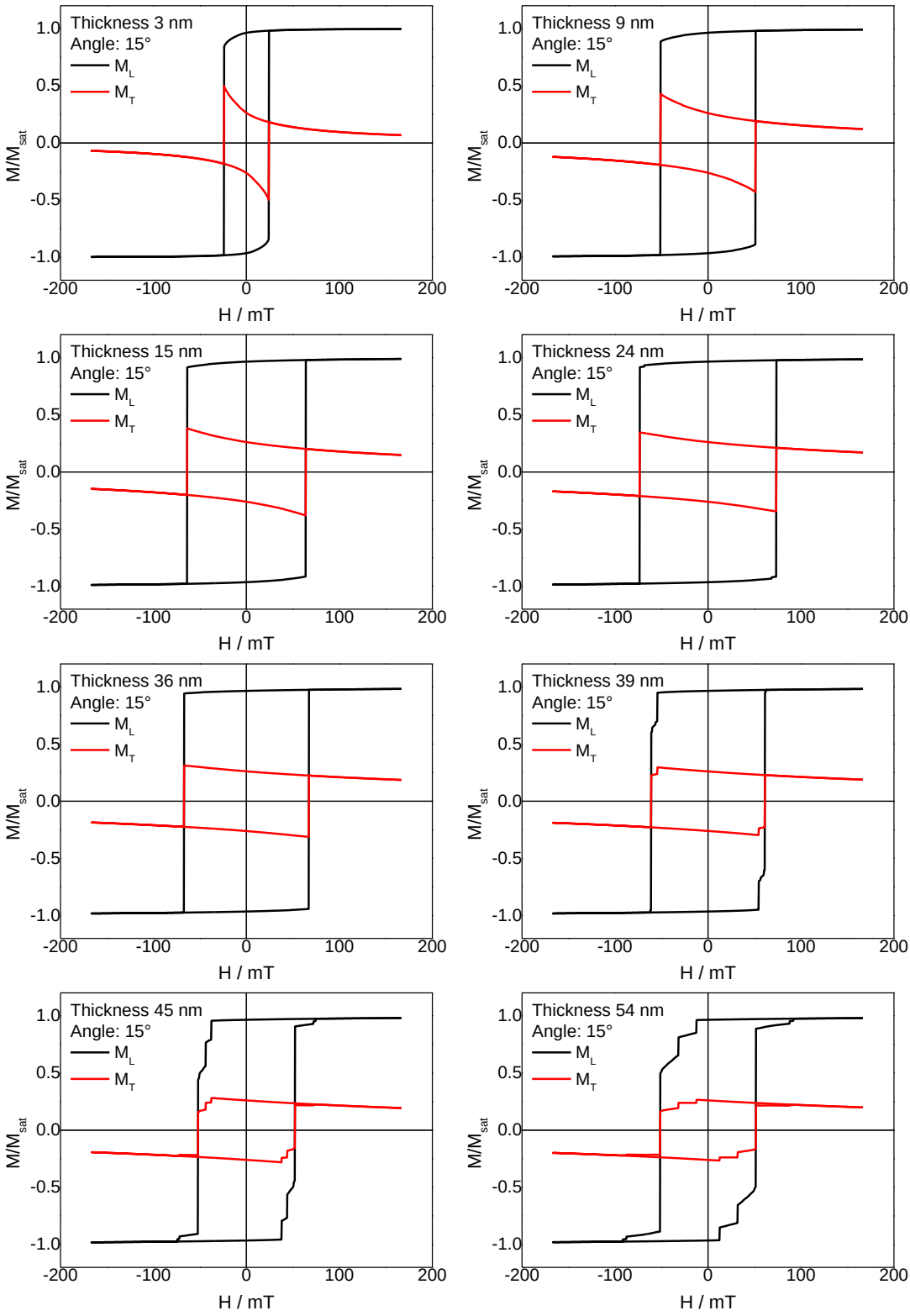

Figure 2. Hysteresis loops of the magnetic nanodot simulated for an angle of 15° with respect to the external magnetic field and different thicknesses.

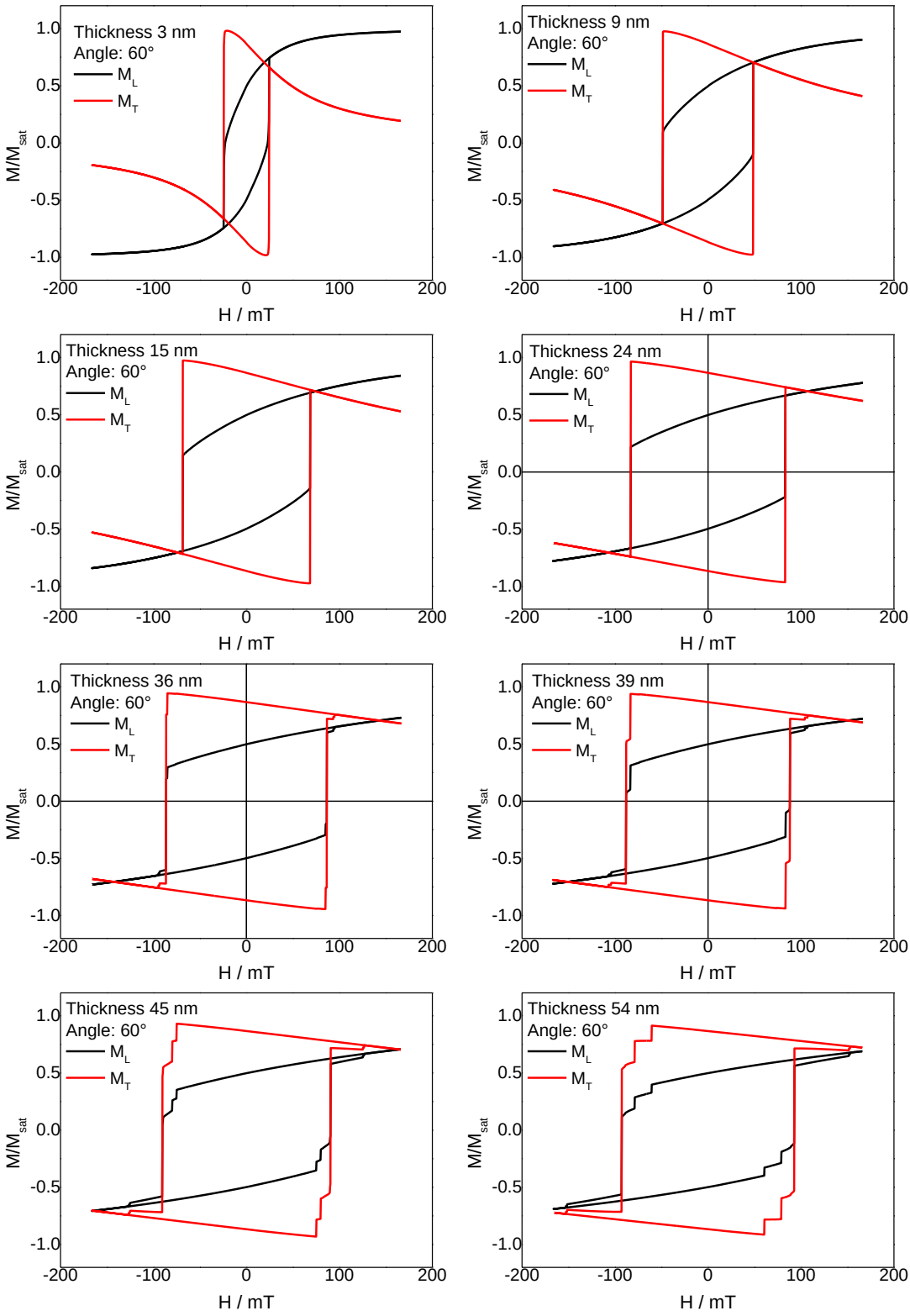

Figure 3. Hysteresis loops of the magnetic nanodot simulated for an angle of 60° with respect to the external magnetic field and different thicknesses.

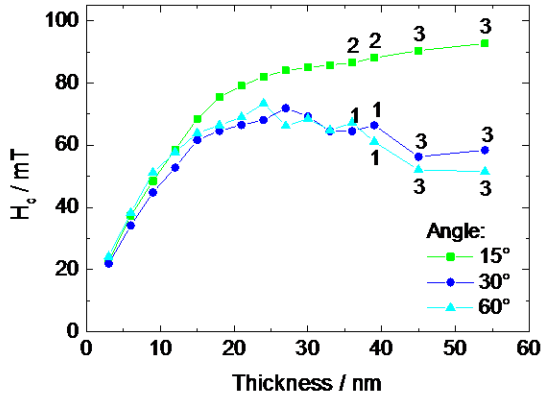

Figure 4. Thickness-dependent coercive fields for different angles between external magnetic field and long sample axis. The numbers indicate the numbers of steps per side of the hysteresis loop, if applicable.

A detailed overview of the coercive fields in dependence on the sample thickness is given in Fig. 4 for different angles with respect to the external magnetic field. Here the already described thickness dependent behaviour of the coercive fields is again visible. While the thickness-dependent coercive fields are similar for smaller thicknesses, they start differing for an angle of 15° for thicknesses above approx. 20 nm. While for an angle of 15°, the coercive fields become larger and larger with increasing thickness, a maximum of the coercive field is reached around an intermediated thickness of approx. 25 nm for the larger magnetic field angles.

The numbers inside the graph, indicating the numbers of steps on each side of the hysteresis loops, becomes larger with increasing sample thickness. This suggests that in thicker samples, magnetization reversal occurs via more than one domain wall process or via different magnetic states, as it is usual, e.g., in square rings from iron [9] or in large enough square or round Fe nanodots with thicknesses of minimum approx. 30 nm [7,8]. While in Fe nanodots, often vortex states dominated for thicker specimens [7,8], here pure vortex states seem impossible due to the elongated sample shape. This is why Figures 5-8 depict the spatially resolved magnetization vectors during a field sweep from positive (along +15° or +60° with respect to the horizontal, respectively) to negative saturation for the maximum and minimum sample thickness investigated here.

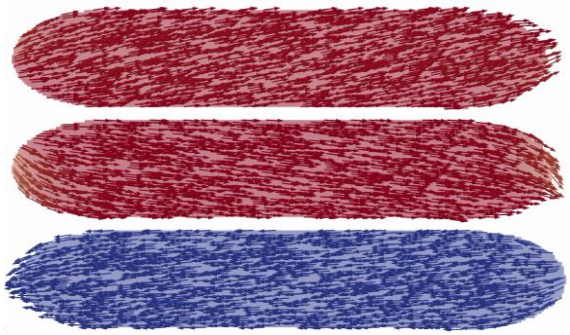

Figure 5. Magnetization reversal from positive to negative saturation for a nanoparticle of thickness 3 nm under an angle of 15° to the external magnetic field.

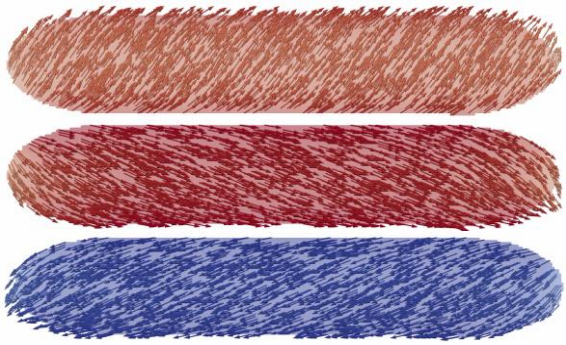

Figure 6. Magnetization reversal from positive to negative saturation for a nanoparticle of thickness 3 nm under an angle of 60° to the external magnetic field.

Fig. 5 shows magnetization reversal of the thinnest sample for an external magnetic field applied under an angle of 15°. During field reduction, the magnetization is more and more aligned along the sample by the shape anisotropy (2nd row), before larger and larger negative magnetic fields finally switch it to negative saturation. Similarly, the magnetization in the sample is firstly relaxed for the 60°

field orientation and afterwards rotated further in one step (coherent magnetization reversal) by applying a larger and larger negative field (Fig. 6). For these thin samples, there are nearly no differences visible for varying external magnetic field orientations.

Magnetization reversal, however, is different for the thickest samples, as depicted in Fig. 4 by the numbers of steps which can be expected to be correlated with domain wall nucleation or other irreversible processes. Fig. 7 depicts the steps of the magnetization reversal process for a sample orientation of 15° to the external magnetic field. Here, magnetization reversal starts with the formation of a vortex at the right side, rotating counter-clockwise (ccw.), followed by a second vortex at the left side, also rotating ccw. The main part of the magnetization in the middle of the sample reversal without destroying the vortices, only the vortex core is shifted to lower the energy necessary for the domain wall between the main part of the magnetization and the part of the vortex rotating oppositely. Magnetization reversal is finished by firstly the right vortex and then the left one disappearing so that magnetization in the whole sample is aligned along the new saturation orientation. Counting these different parts of the magnetization reversal process actually results in four steps in addition to the main magnetization reversal step, while Fig. 4 only announced 3 steps. Comparing the processes visible in Fig. 7 with the hysteresis loops given in Fig. 2 shows that apparently the two steps after the main switching process, i.e. vanishing of the vortices, cannot be recognized in the hysteresis loops at different steps.

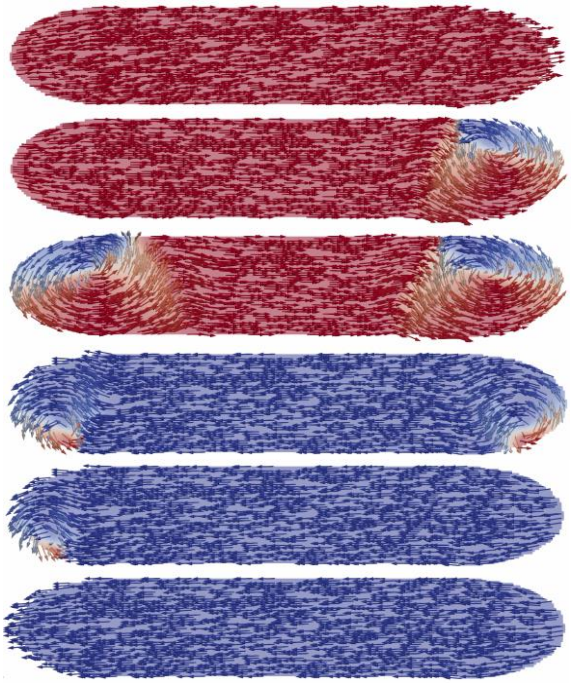

Figure 7. Magnetization reversal from positive to negative saturation for a nanoparticle of thickness 54 nm under an angle of 15° to the external magnetic field.

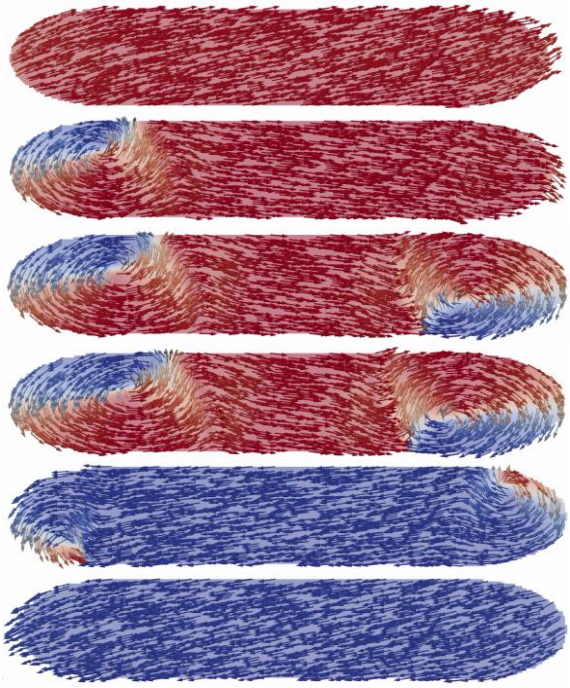

Figure 8. Magnetization reversal from positive to negative saturation for a nanoparticle of thickness 54 nm under an angle of 60° to the external magnetic field.

For an angle of 60° (Fig. 8), the process is quite similar. Here, however, the left vortex becoming visible firstly rotates again ccw., while the second vortex on the right side now rotates clockwise (cw.). In addition, for a short period of time, both vortices can be recognized moving to each other, before the main magnetization area in the middle switches, and the vortices jump back to the outer edges. Finally, they both switch at the same external magnetic field.

4. Conclusion

Magnetization reversal processes were investigated for an elongated nanodot, combining the usually investigated shapes of a cylindrical nanodot and a rectangle. Depending on the thickness, magnetization reversal works via coherent rotation – in case of thin particles – or via vortex nucleation at the ends. The number of possible reversal mechanisms is thus strongly reduced, as compared to round or flat nanodots of different thickness [7,8]. This finding suggests testing similar systems with varying length of the inner rectangular area to investigate for which lengths of length-to-width ratios how many vortices occur, and whether for longer rectangular areas, additional domain walls may occur along the rectangular part, as it is known from pure rectangles.

5. References

[1] Li H J, Wu Q, Yue M, Peng Y, Li Y Q, Liang J M, Wang D J, Zhang J X 2019 *J. Magn. Magn. Mater.* **481** 104-110
[2] Gao X S, Adeyeye A O, Goolaup S, Singh N, Jung W, Castano F J, Ross C A 2007 *J. Appl. Phys.* **101** 09F505
[3] Vavassori P, Bovolenta R, Metlushko V, Ilic B 2006 *J. Appl. Phys.* **99** 053902
[4] Leong T G, Zarafshar A M, Gracias D H 2010 *Small* **6** 792
[5] Amaladass E, Ludescher B, Schütz G, Tyliszczak T, Lee M-S, Eimüller T 2010 *J. Appl. Phys.* **107** 053911
[6] Schneider V, Reinholdt A, Kreibig U, Weirich T, Güntherodt G, Beschoten B, Tillmanns A, Krenn H, Rumpf K, Granitzer P 2006 *Z. Phys. Chem*. **220** 173-187
[7] Ehrmann A, Blachowicz T 2018 *Hyperfine Interactions* **239** 8
[8] Ehrmann A, Blachowicz T 2018 *J. Magn. Magn. Mater.* **475** 727-733
[9] Blachowicz T, Ehrmann A, Steblinski P and Palka J 2013 *J. Appl. Phys.* **113** 013901
[10] Zhang W and Haas S 2010 *Phys. Rev. B* **81** 064433
[11] Zhu F Q, Fan D L, Zhu X C, Zhu J G, Cammarata R C, Chien C L 2004 *Adv. Mater.* **16**, 2155
[12] Faulkner C C, Cooke M D, Allwood D A, Petit D, Atkinson D, Cowburn R P 2004 *J. Appl. Phys.* **95** 6717-6719
[13] Munjal S, Khare N 2018 *Appl. Phys. Lett.* **113** 243501
[14] Alawein M, Amara S, Fariborzi H 2019 *IEEE Magn Lett* **10** 6102005
[15] Grollier J, Boullenc P, Cros V, Hamzic A, Vaurès A, Fert A and Faini G 2003 *Appl. Phys. Lett.* **83** 509
[16] Vernier N, Allwood D A, Atkinson D, Cooke M D, Cowburn R P 2004 *Europhys. Lett.* **65** 526-532
[17] Yang S-H, Ryu K-S, Parkin S S P 2015 *Nat. Nanotechnol.* **10** 221-226
[18] Blachowicz T, Ehrmann A 2018 *J. Appl. Phys.* **124** 152112
[19] Garg C, Yang S-H, Phung T, Pushp A, Parkin S S P 2017 *Sci. Adv.* **3** e1602804
[20] Moreno R, Carvalho-Santos V L, Espejo A P, Laroze D, Chubykalo-Fesenko O, Altbir D 2017 *Phys. Rev. B* **96** 184401
[21] Schumm R D, Kunz A 2016 Appl. Phys. Lett. **109** 202405
[22] Kern P, Döpke C, Blachowicz T, Steblinski P, Ehrmann A 2019 *J. Magn. Magn. Mater.* **484** 37-41
[23] Donahue M J, Porter D G 1999 OOMMF User's Guide, Version 1.0 Interagency Report NISTIR 6376. National Institute of Standards and Technology, Gaithersburg
[24] Kneller E F and Hawig R 1991 *IEEE Trans. Magn.* **27** 3588
[25] Blachowicz T, Ehrmann A 2011 *J. Appl. Phys.* **110** 073911
[26] Stoner E C and Wohlfarth E P 1948 *Phil. Trans. Royal Soc. A* **240** 599-642

Acknowledgments

This work was supported by Volkswagen Foundation grant "Adaptive Computing with Electrospun Nanofiber Networks" no. 93679.